Silica nanoparticles-coated poly(glycidyl methacrylate-ethylene dimethacrylate) co-polymer beads containing organic phase change materials

Tivadar Feczkó[a,b*], László Trif[a], Bence Németh Trif[b], Daniel Horák[c]

[a]Institute of Materials and Environmental Chemistry, Research Centre for Natural Sciences, Hungarian Academy of Sciences, Magyar tudósok körútja 2., 1117, Budapest, Hungary

[b]Research Institute of Chemical and Process Engineering, Faculty of Information Technology, University of Pannonia, Egyetem u. 10, H-8200 Veszprém, Hungary

[c]Institute of Macromolecular Chemistry, Academy of Sciences of the Czech Republic, Heyrovsky Sq. 2, 16206 Prague 6, Czech Republic

* E-mail: tivadar.feczko@gmail.com, phone: +36-88-623508, fax: +36-88-624038

Abstract

Macroporous sorbent beads of large and small sizes were prepared by the AIBN-initiated suspension radical polymerization of glycidyl methacrylate and ethylene dimethacrylate monomers in the presence of an inert porogen. The large and small microspheres were loaded with paraffin and cetyl alcohol PCMs, respectively, and coated with silica nanoparticles after sol-gel synthesis of trimethoxy(methyl)silane hydrolysate. The energy storing capacity of the form-stabilized PCM containing composite particles was monitored by differential scanning calorimetry. Accelerated thermal cycling tests were carried out to determine the thermal reliability of the microencapsulated PCMs. Paraffin and cetyl alcohol content of the microcapsules was 42.9 % and 48.9 %, respectively. The microcomposites with higher PCM content showed correspondingly higher latent heat storage capacity (melting and solidification enthalpies were 96.1 J/g and 94.7 J/g). However, there was low enthalpy change observed after 1000 thermal cycles of cetyl alcohol containing capsules, which indicated that its leakage from the microcomposites was not substantial.

Keywords: porous poly(glycidyl methacrylate-ethylene dimethacrylate) beads, paraffin and cetyl alcohol phase change materials, silica nanoparticles shell.

1 Introduction

Thermal energy storage has received more and more attention during the past decades due to the endeavour of energy saving. Latent heat storage is one of the most efficient ways of storing thermal energy. The main benefits of latent heat storage compared with that of sensible heat are the much higher storage density accompanying with a smaller temperature difference between storing and releasing heat. Phase change materials (PCMs) are used for latent heat storage. Most promising applications of PCMs are waste heat recovery systems, solar heating systems, building energy conservation systems and air-conditioning systems. Most of the organic PCMs are non-corrosive and chemically inert, stable, recyclable and compatible with numerous building materials. They have desirable cohesion, a high latent heat per unit weight, low vapour pressure, no supercooling, and offer congruent melting and self-nucleation. They have disadvantages such as low thermal conductivities, flammability and high changes in volume during phase change. In

order to overcome these problems, their microencapsulation can be an efficient tool. Microencapsulation process is the entrapment of PCMs in natural and synthetic polymeric capsules. The advantages of the microencapsulated PCMs are the protection of PCM against the environmental effects, the enhancement of the specific heat-transfer area, and the elimination of the volume change of PCM during phase change by providing void space [1].

Most frequently applied microencapsulation techniques of organic PCMs are simple coacervation, in situ polymerization of e.g. methacrylate [1,2], other acrylic polymers [3] or melamine–formaldehyde [4], however, emulsion methods/phase separation [5,6] and interfacial coacervation and crosslinking [7] can be also efficient to prepare PCM containing capsules of core-shell structure.

Organic/inorganic composite form-stable phase change materials combine the advantages of the inorganic and the organic components [8,9]. The inorganic supporting material provides structural strength and prevents the leakage of the organic PCM component. Several preparation methods of the organic/inorganic composite form-stable phase change materials were described. The most important ones are absorption [8,10], solution intercalation [11] and sol–gel method [12,13]. Among them, the main benefit of the sol–gel method is the simplicity and low cost

In the present work, the form-stabilization of PCM was achieved by imbedding cetyl alcohol or paraffin in porous poly(glycidyl methacrylate-ethylene dimethacrylate) (P(GMA-EDMA)) beads, and the leakage of PCM was prevented by a shell composed of silica nanoparticles prepared by sol-gel method. The carrier beads synthesized from this copolymer by suspension radical polymerization have not been used as support for PCMs so far. However, Chen et al. [14] covalently bound poly(glycidyl methacrylate) (PGMA) to polyethylene glycol PCM through the ring-opening crosslinking reaction of end-carboxyl groups of carboxyl polyethylene glycol and epoxy groups in PGMA.

2 Experimental

2.1 Materials

Glycidyl methacrylate (GMA; Aldrich; St. Louis, MO, USA) and ethylene dimethacrylate (EDMA; Ugilor S.A., France) were distilled before use under reduced pressure. 2,2′-Azobis(isobutyronitrile)   (AIBN;   recrystallized   from   ethanol),   [(2-

hydroxypropyl)methyl]cellulose (Methocel 90 HG), (2-hydroxyethyl)cellulose, poly(*N*-vinyl-2-pyrrolidone) K 90 (PVP; M_w = 360,00) and cetyl alcohol (CA) and were obtained from Fluka (Buchs, Switzerland), poly(vinyl alcohol) (PVA; Polyviol W 25/140; M_w = 80,000) from Wacker (Germany). Trimethoxy(methyl)silane (TMMS) and Tween 20 were from Sigma-Aldrich and paraffin (P), melting-solidification range 53-55 °C, from Paramo (Pardubice, Czech Republic). Other chemicals and solvents were purchased from Lachner (Neratovice, Czech Republic).

2.2 Synthesis of macroporous beads

Macroporous sorbent beads were prepared by the AIBN-initiated suspension radical polymerization of GMA and EDMA using an inert porogen [15]. Aqueous 0.2 wt.% PVP, 0.2 wt.% hydroxyethyl cellulose and 0.006 wt.% PVA solution (6 l) formed the continuous phase, while the dispersed phase consisted of GMA (480 g), EDMA (320 g), AIBN (4 g) and porogen. The porogen was composed of the mixture of toluene (885 g) and 1,2-dichloroethane (315 g) or that of cyclohexanol (1180 g) and dodecan-1-ol (20 g). The reaction mixture was stirred at 90 rpm and heated to 75 °C for 6 h. The resulting beads were washed with water, toluene and methanol.

2.3 Loading of phase change materials in the beads and formation of silica nanoparticles shell

Macroporous beads (2 g) were dispersed in molten cetyl alcohol (5 g) or paraffin (5 g) which were loaded at 65-100 °C. The particles were separated by centrifugation using a stainless sieve and again dispersed in aqueous 0.1 wt.% Methocel 90 HG solution (20 ml) at 70 °C in 50-ml reaction vessel under stirring with an anchor-type stirrer (500 rpm).

TMMS (1.36 g; 10 mmol) was hydrolyzed in 0.01 M HCl (0.54 g; 30 mmol) at room temperature to yield $SiMe(OR)_3$ hydrolysate. The volume of the mixture was adjusted to 5 ml by adding distilled water. The TMMS hydrolysate (1 ml) was added to the resulting poly(glycidyl methacrylate-ethylene dimethacrylate)-phase change material (P(GMA-EDMA)-PCM) beads, the suspension was stirred at 70 °C for 3.5 h and the product eight times washed in 0.01 wt.% Tween 20 (100 ml each). Finally, the poly(glycidyl methacrylate-ethylene dimethacrylate)-phase change material-methyl silica particles (P(GMA-EDMA)-PCM-Me-SiO_2) were dried in air.

2.4 Characterization methods

Carl Zeiss optical microscope (Germany) and Philips XL-30 environmental scanning electron microscope (ESEM) operated at 25 kV were used for the imaging of the particles. The size distribution of the beads was measured by a Mastersizer 2000 (Malvern Instruments, Malvern, UK) applying laser diffraction method.

The specific surface area (S_{BET}) of the microspheres was determined by nitrogen adsorption (77 K) using a Gemini VII 2390 Analyzer (Micromeritics; Norcross, GA, USA). Pore volume was determined from cyclohexane or 1-chlorododecane regain using centrifugation method [16]. The PCM content of the beads was calculated after weighing 100 mg of the beads, and extracting the PCM 3 times from the microcapsules by each 5 ml n-hexane.

The thermal properties of the microcapsules were determined by a Setaram μDSC3evo differential scanning microcalorimeter. The samples were weighed into 100 μl aluminium crucibles, and ethylene glycol as a heat transferring medium was added, which covered the microparticles, and then the system was closed by crimping a cap. The samples were cycled with a scanning rate of 0.6 °C/min. The results were processed by the thermoanalyzer's Calisto Processing (v1.38) software. The corresponding melting/freezing enthalpies and onset temperatures were determined by the baseline integration method (Tangential sigmoid baseline type).

The covered beads were tested via accelerated thermal cycling in order to study whether they are capable to retain the PCM after several phase transition. One thermal cycling test included heating until the complete melting and cooling until the complete freezing of the phase change materials in the capsules. The tests were performed consecutively up to 1000 thermal cycles by heating and cooling using a Peltier element. DSC analysis was repeated after the thermal cycling using a Setaram μDSC3evo.

3 Results and Discussion

3.1 Porosity, size and PCM content

Macroporous sorbent beads were prepared by the AIBN-initiated suspension radical polymerization of GMA and EDMA in the presence of an inert porogen. The porogen for the bead preparation was a mixture of toluene/1,2-dichloroethane and cyclohexanol/dodecan-1-ol, respectively. While the former mixture was preferred for preparation of large particles, the latter

one was suitable for synthesis of small beads. Copolymerization of GMA (60 wt.%) with EDMA (40 wt.%) produced particles possessing reactive oxirane groups. Two types of beads were thus obtained: large (P(GMA-EDMA)L) and small microspheres (P(GMA-EDMA)S). Both of the small and large beads had moderate specific surface area and pore volume, and these properties did not show significant difference (Table 1).

The P(GMA-EDMA) beads were rather hydrophobic, i.e., compatible (well wettable) with the PCMs, which facilitated their fast imbibition, filling of the pores and air displacement thanks to the low interfacial tension. The large and the small beads were filled with paraffin and cetyl alcohol PCMs, respectively. After PCM loading, the particles were dispersed in the [(2-hydroxypropyl)methyl]cellulose solution and via hydrolysis and condensation of silane, a shell of silica nanoparticles was formed in sol-gel process of TMMS hydrolysate. Silica nanoparticles formed on the surface of the beads can be noticed in the SEM images of the surface of the beads (Fig. 1). Both of the large and the small microcapsules had spherical shape (Fig. 2).

The large particles loaded with paraffin PCM and covered by silica nanoparticles were 300-1400 μm in size (average size: 643 μm), while the small beads with cetyl alcohol and silica nanosphere shell ranged between 70 and 200 μm (average size: 111 μm) (Fig. 3, Table 2)

Although the specific surface area and the pore volume of the large and small beads were very similar (Table 1), the PCM content of the small beads was substantially higher than that of the large beads (Table 2). The reason for this finding is probably that the cetyl alcohol-copolymer interaction is more favourable than the adsorption of paraffin to the carrier of the same composition.

3.2 DSC analysis

Thermal properties of the PCM containing composites were studied by DSC measurements. The thermal energy storage capacity of pure paraffin and cetyl alcohol can be followed in Fig. 4a and Fig. 4b, respectively. The melting and crystallizing enthalpies of the P(GMA-EDMA)-P-Me-SiO$_2$ composite was found to be 77.6 J/g and 78.7 J/g (Fig. 3c), respectively, which were slightly lower than the value that could be calculated from their paraffin content (42.9 %). This difference might be explained by the thermal isolating effect of the silica shell. The melting and solidifying latent heats of P(GMA-EDMA)-CA-Me-SiO$_2$ microcapsules were 96.1 J/g and 94.7 J/g, respectively.

These values were a bit lower again related to the ones which can be determined from their PCM content (48.9 %). The latent heat storage capacity of our developed composites is comparable with the form-stabilized PCMs that have already been prepared from similar types of carriers or with similar procedure. E.g. the thermal energy storage capacity of polyethylene glycol PCM crosslinked with PGMA was around 70 J/g [14]. Microencapsulated palmitic acid (PA) with titanium dioxide (TiO_2) shell as shape-stabilized thermal energy storage material was formed through a sol–gel process. The microcapsules melted with a latent heat of 63.3 J/g and solidified with a latent heat of 47.1 J/g [17].

3.3 Thermal reliability

In order to test whether the PCM leakage was avoided efficiently, 1000 heating and subsequent cooling cycles of the capsules were performed. The heat storage capacity of the PCM containing capsules was investigated by DSC. The melting and crystallizing enthalpies of cetyl alcohol (Fig 5B) containing composites decreased slightly, although the heat storage capacity reduction of paraffin containing silica covered beads (Fig 5A) was not negligible.

This result verifies that the cetyl alcohol adsorption is stronger to the copolymer than that of the paraffin. It can also be concluded that the shell of silica nanoparticles could not completely inhibit the leakage of the PCMs.

4 Conclusions

Large and small macroporous poly(glycidyl methacrylate-ethylene dimethacrylate) beads were synthesized by the suspension polymerization technique and imbibed with high amount of paraffin and cetyl alcohol phase change materials. The PCM-loaded beads were coated with a protective shell of silica nanoparticles via sol-gel synthesis from trimethoxy(methyl)silane hydrolysate. According to the results obtained by differential scanning calorimetry, both of the composites showed high latent heat storage capacity. Due to the higher cetyl alcohol content, which was the result of its higher affinity to the carrier copolymer, larger melting and solidifying enthalpies were measured compared to those values found for paraffin containing coated beads. The beneficial latent heat storage capability of the former one could be preserved more effectively after the thermal cycling tests.

7

Acknowledgement

References

[1] Sari A, Alkan C, Karaipekli A, Uzun O (2009) Microencapsulated n-octacosane as phase change material for thermal energy storage. Sol Energ 83:1757-1763.

[2] Ma S, Song G, Wei L, Fan P, Tang G (2010) UV irradiation initiated MMA polymerization to prepare microcapsules containing phase change paraffin. Sol Energy Mater Sol Cells 94:1643–1647.

[3] Qiu X, Song G, Chu X, Li X, Tang G (2013) Microencapsulated n-alkane with p(n-butyl methacrylate-*co*-methacrylic acid) shell as phase change materials for thermal energy storage. Sol. Energ 91:212-220.

[4] Wei L, Zhang XX, Wang XC, Niu JJ (2007) Preparation and characterization of microencapsulated phase change material with low remnant formaldehyde content. Mater Chem Phys 106:437–442.

[5] Loxley A, Vincent B (1998) Preparation of poly(methylmethacrylate) microcapsules with liquid cores. J Colloid Interf Sci 208:49–62.

[6] Feczkó T, Kardos FA, Németh B, Trif L, Gyenis J (2014) Microencapsulation of n-hexadecane phase change material by ethyl cellulose polymer. Polym Bull 71:3289-3304.

[7] Németh B, Németh ÁS, Tóth J, Fodor-Kardos A, Gyenis J, Feczkó T (2015) Consolidated microcapsules with double alginate shell containing paraffin for latent heat storage. Sol Energy Mater Sol Cells (in press).

[8] Sari A, Karaipekli A (2009) Preparation, thermal properties and thermal reliability of palmitic acid/expanded graphite composite as form-stable PCM for thermal energy storage. Sol Energy Mater Sol Cells 93:571–576.

[9] Tang B, Cui J, Wang Y, Jia C, Zhang S (2013) Facile synthesis and performances of PEG/SiO2 composite form-stable phase change materials. Sol Energ 87:484-492.

[10] Nomura T, Okinaka N, Akiyama T (2009) Impregnation of porous material with phase change material for thermal energy storage. Mater Chem Phys 115:846–850.

[11] Fang X, Zhang Z, Chen Z (2008) Study on preparation of montmorillonite-based composite phase change materials and their applications in thermal storage building materials. Energy Convers Manage 49:718–723.

[12] Lana SLB, Seddon AB (1998) X-Ray diffraction studies of sol-gel derived ORMOSILs based on combinations of tetramethoxysilane and trimethoxysilane. J Sol-Gel Sci Technol 13:461–466.

[13] Oulkadi D, Desobry S, Mustin C, Desobry-Banon S (2012) Water sorption in hybrid silica gels containing colloidal nontronite. J Sol-Gel Sci Technol 64:653–660.

[14] Chen CZ, Liu WM, Yang H, Zhao Y, Liu S (2011) Synthesis of solid-solid phase change material for thermal energy storage by crosslinking of polyethylene glycol with poly(glycidyl methacrylate). Sol Energ 88:2679-2685.

[15] Grama S, Boiko N, Bilyy R, Klyuchivska O, Antonyuk V, Stoika R, Horak D (2014) Novel fluorescent poly(glycidyl methacrylate) - silica microspheres. Europ Polym J 56:92-104.

[16] Stamberg J, Sevcik S (1966) Chemical transformations of polymers. 111. Selective hydrolysis of a copolymer of diethylene glycol methacrylate and diethylene glycol dimethacrylate. Collect Czechoslov Chem Commun 31:1009-1016.

[17] Cao L, Tang F, Fang G (2014) Preparation and characteristics of microencapsulated palmitic acid with TiO2 shell as shape-stabilized thermal energy storage materials. Sol Energy Mater Sol Cells 123:183-188.

Table 1 Specific surface area (m^2/g) and pore volume (m^2/g) of large (L) and small (S) P(GMA-EDMA) beads.

	S_{BET} (m^2/g)	V (m^2/g)
P(GMA-EDMA)L	63	2.6
P(GMA-EDMA)S	64	2.5

Table 2 Volume mean diameter (μm) and PCM content (%) of P(GMA-EDMA) beads containing cetyl alcohol (CA) and paraffin (P) phase change materials, both covered by silica shell.
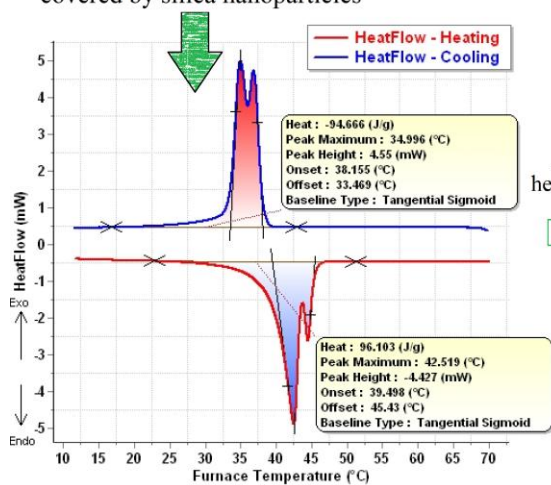
PCM	Volume mean diameter (μm)	PCM content (%)
P(GMA-EDMA)-P-SiO$_2$	643	42.9
P(GMA-EDMA)-CA-SiO2	111	48.9

Graphical abstract
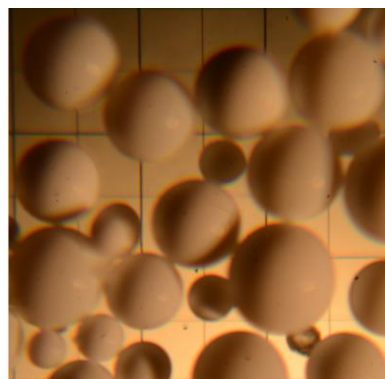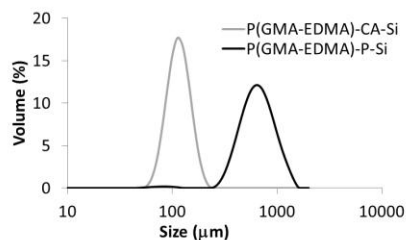
Small beads filled with cetyl alcohol
covered by silica nanoparticles

Large beads filled with paraffin
covered by silica nanoparticles
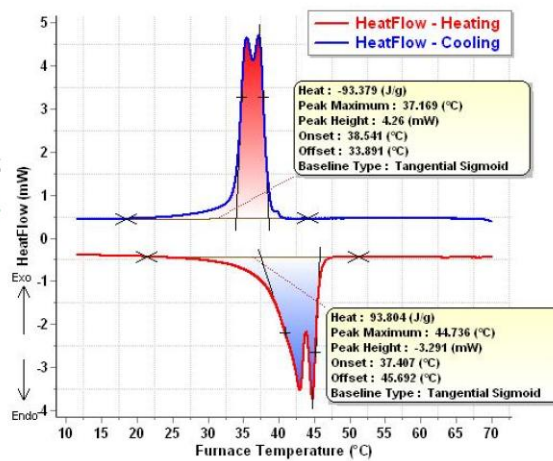
After 1000
heating-cooling

Figure captions:

Fig. 1 Surface of P(GMA-EDMA) beads containing paraffin (A) and cetyl alcohol (B) phase change materials and covered with silica shell by SEM

Fig. 2 Optical micrographs of P(GMA-EDMA) beads containing paraffin (A) cetyl alcohol (B) and shell of silica nanoparticles. Squares indicate size of 0.5x0.5 mm

Fig. 3 Size distribution of P(GMA-EDMA)-CA-SiO$_2$ and P(GMA-EDMA)-P-SiO$_2$

Fig. 4 DSC of paraffin (A), cetyl alcohol (B), P(GMA-EDMA)-P-SiO$_2$ (C) and P(GMA-EDMA)-CA-SiO$_2$ (D)

Fig. 5 DSC of P(GMA-EDMA)-P-SiO$_2$ (A) and P(GMA-EDMA)-CA-SiO$_2$ (B) after 1000 heating-cooling cycles

Fig.1a

Acc.V Spot Magn   Det WD   Exp   5 μm
25.0 kV 3.0 5000x   BSE 9.7   70385   PC 60
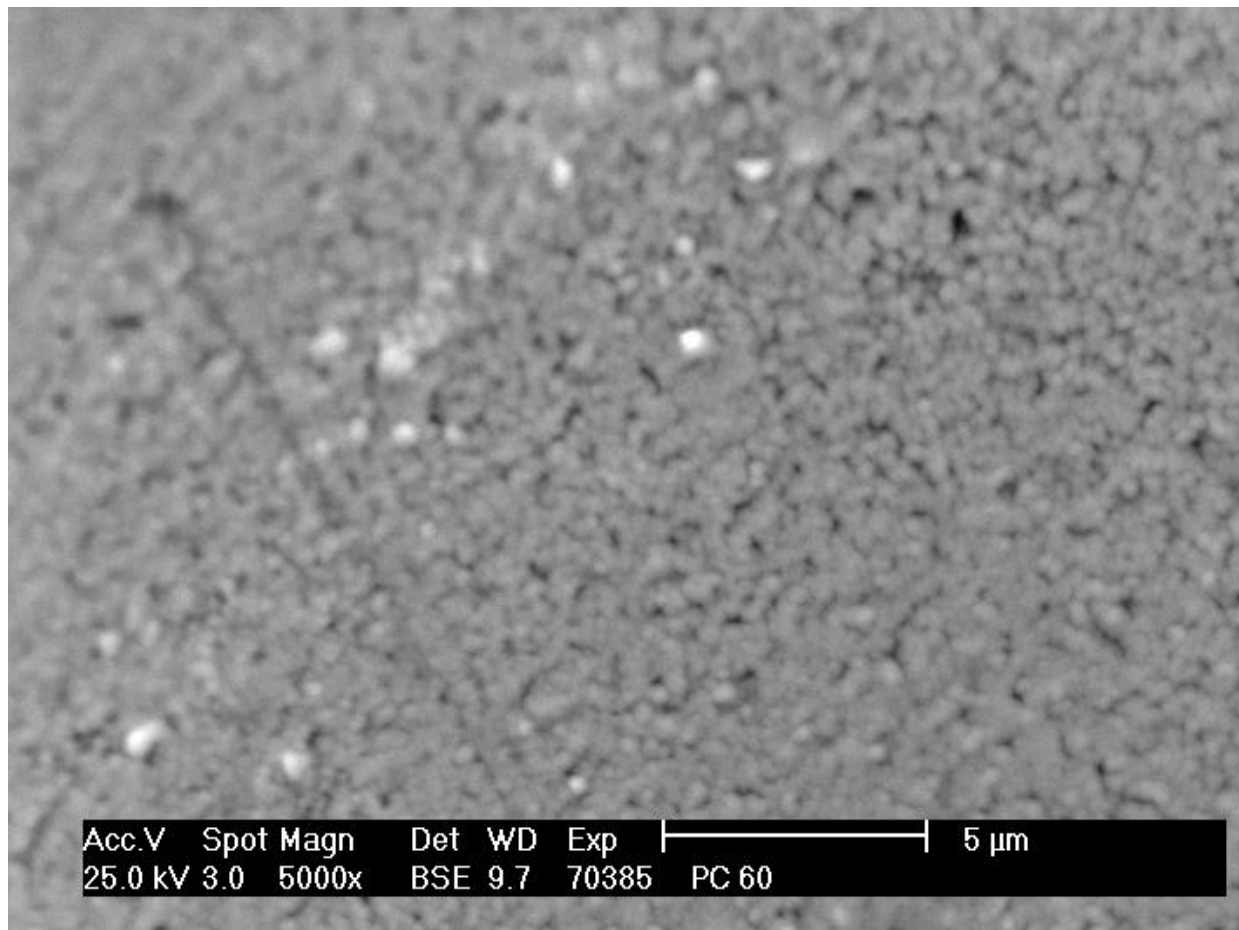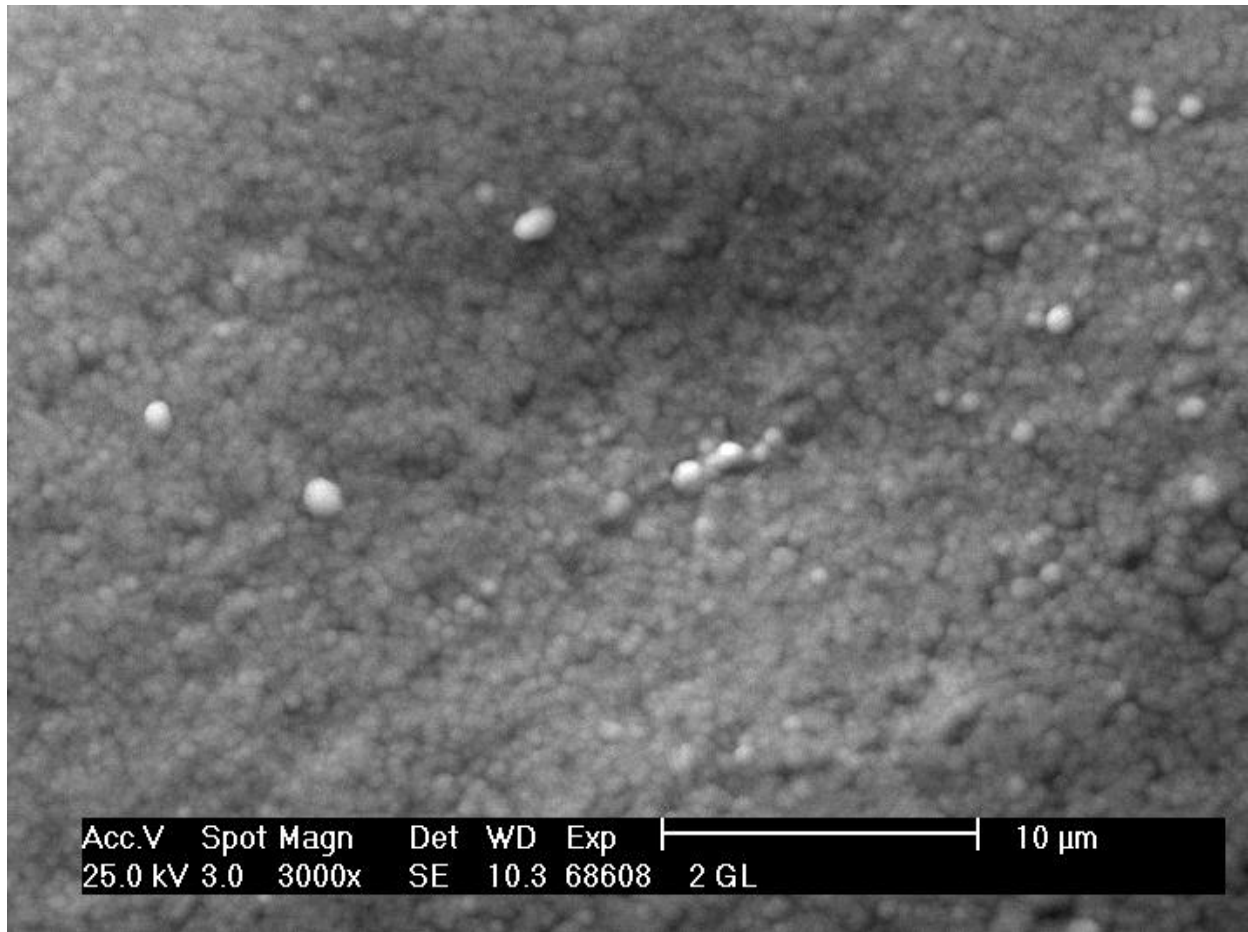
Fig.1b

Acc.V Spot Magn Det WD Exp   10 µm
25.0 kV 3.0 3000x SE   10.3 68608 2 GL

Fig.2a

Fig.2b

Fig.3

Figure showing Volume (%) versus Size (μm) distribution curves for P(GMA-EDMA)-CA-Si and P(GMA-EDMA)-P-Si.

Fig.4a

Heat : -199.933 (-158.71 -41.222) (J/g)
Peak Maximum : 53.671 (℃)
Peak Maximum 2 : 34.548 (℃)
Peak Height : 3.978 (mW)
Peak Height 2 : 0.716 (mW)
Onset : 55.064 (℃)
Offset : 26.911 (℃)
Baseline Type : Tangential Sigmoid

Heat : 203.488 (44.55 + 158.938) (J/g)
Peak Maximum : 37.12 (℃)
Peak Maximum 2 : 54.62 (℃)
Peak Height : -0.762 (mW)
Peak Height 2 : -3.805 (mW)
Onset : 30.034 (℃)
Offset : 57.425 (℃)
Baseline Type : Tangential Sigmoid

HeatFlow - Heating
HeatFlow - Cooling

HeatFlow (mW)
Exo
Endo

Furnace Temperature (°C)

Fig.4b

Legend / annotations within figure:

HeatFlow - Heating
HeatFlow - Cooling

Heat : -218.032 (0.00E+0 -218.032) (J/g)
Peak Maximum : 49.17 (°C)
Peak Maximum 2 : 40.909 (°C)
Peak Height : 0.00E+0 (mW)
Peak Height 2 : 10.927 (mW)
Onset : 47.439 (°C)
Offset : 39.998 (°C)
Baseline Type : Tangential Sigmoid

Heat : 204.273 (J/g)
Peak Maximum : 49.651 (°C)
Peak Height : -10.585 (mW)
Onset : 48.159 (°C)
Offset : 50.462 (°C)
Baseline Type : Tangential Sigmoid

Y-axis: HeatFlow (mW), Exo ↑, Endo ↓
X-axis: Furnace Temperature (°C)

Fig.4c

Heat : -78.686 (J/g)
Peak Maximum : 53.396 (°C)
Peak Height : 2.1 (mW)
Onset : 54.842 (°C)
Offset : 28.964 (°C)
Baseline Type : Tangential Sigmoid

Heat : 77.604 (J/g)
Peak Maximum : 55.279 (°C)
Peak Height : -2.016 (mW)
Onset : 29.843 (°C)
Offset : 56.633 (°C)
Baseline Type : Tangential Sigmoid

20

Fig.4d

Heat : -94.666 (J/g)
Peak Maximum : 34.996 (°C)
Peak Height : 4.55 (mW)
Onset : 38.155 (°C)
Offset : 33.469 (°C)
Baseline Type : Tangential Sigmoid

Heat : 96.103 (J/g)
Peak Maximum : 42.519 (°C)
Peak Height : -4.427 (mW)
Onset : 39.498 (°C)
Offset : 45.43 (°C)
Baseline Type : Tangential Sigmoid

Fig.5a

Fig.5b

Heat : -93.379 (J/g)
Peak Maximum : 37.169 (°C)
Peak Height : 4.26 (mW)
Onset : 38.541 (°C)
Offset : 33.891 (°C)
Baseline Type : Tangential Sigmoid

Heat : 93.804 (J/g)
Peak Maximum : 44.736 (°C)
Peak Height : -3.291 (mW)
Onset : 37.407 (°C)
Offset : 45.692 (°C)
Baseline Type : Tangential Sigmoid